

Primordial Star Formation under Far-Ultraviolet Radiation

Kazuyuki Omukai

*Division of Theoretical Astrophysics, National Astronomical Observatory, Mitaka, Tokyo
181-8588, Japan*

omukai@th.nao.ac.jp

ABSTRACT

Thermal and chemical evolution of primordial gas clouds irradiated with far-ultraviolet (FUV; $h\nu < 13.6$ eV) radiation is investigated. In clouds irradiated by intense FUV radiation, sufficient hydrogen molecules to be important for cooling are never formed. However, even without molecular hydrogen, if the clouds are massive enough, they start collapsing via atomic hydrogen line cooling. Such clouds continue to collapse almost isothermally owing to successive cooling by H^- free-bound emission up to the number density of 10^{16}cm^{-3} . Inside the clouds, the Jeans mass eventually falls well below a solar mass. This indicates that hydrogen molecules are dispensable for low-mass primordial star formation, provided fragmentation of the clouds occurs at sufficiently high density.

Subject headings: cosmology: theory — early universe — galaxy formation — molecular processes — stars: formation

1. Introduction

Since the dawn of evolutionary cosmology, great efforts toward understanding the formation of the first structures have been made by many authors (e.g., Saslaw & Zipoy 1967; Peebles & Dicke 1968; Matsuda, Sato, & Takeda 1969; Doroshkevich & Kolesnik 1976; Carlberg 1981; Palla, Salpeter, & Stahler 1983; Kashlinsky & Rees 1983). In particular, partly stimulated by observational advances and by the consequent detectability of the first stars by next-generation facilities, this area is being vigorously investigated these days (e.g., Haiman, Thoul, & Loeb 1996; Ostriker & Gnedin 1996; Tegmark et al. 1997; Yamada & Nishi 1998; Bromm, Coppi, & Larson 1999; Abel, Bryan, & Norman 2000; Fuller & Couchman 2000). Those studies have repeatedly emphasized the key role played by molecular hydrogen.

The role of H_2 in the cosmological context is twofold. First, small primordial clouds whose virial temperature is $1000 \lesssim T_{\text{vir}} \lesssim 8000\text{K}$ can cool and start collapsing via H_2 line cooling after virialization (e.g., Haiman et al. 1996). Second, the Jeans mass inside a collapsing primordial cloud

is eventually reduced to much less than a solar mass as a result of H₂ cooling (e.g., Palla et al. 1983).

Regarding the former role, there is some dispute over the role of H₂ in the formation of second-generation stars, namely, what happens after the first stars have formed by H₂ cooling. Formed first stars or first quasars can be sources of UV radiation. Whereas ionizing photons are trapped in an HII region around the source, far-ultraviolet (FUV; $h\nu < 13.6$ eV) photons¹ travel farther and form an outer H₂ photodissociation region (PDR). Therefore, before the overlap of the HII regions, or in other words the reionization of the universe, the H₂ PDRs must cover the whole intergalactic space. At that time, the universe is filled with FUV background radiation (e.g., Haiman, Rees, & Loeb 1997; Ciardi, Ferrara, & Abel 2000).

Hydrogen molecules in small objects can easily be photodissociated by either internal or external UV sources. Haiman et al. (1997) found that in the presence of UV background radiation at the level needed to reionize the universe, molecular hydrogen is photodissociated in small cosmological objects. Furthermore, Omukai & Nishi (1999) pointed out that even a single O star formed in a small cosmological object is able to photodissociate the whole original cloud. In addition, those clouds are easily blown out by a few supernovae because of their shallow potential wells (e.g., Mac Low & Ferrara 1999). These effects strongly regulate the subsequent star formation within small pregalactic clouds.

In contrast to this, the temperature of sufficiently massive clouds reaches above ~ 8000 K, where atomic Ly α emission begins to be an effective cooling agent. Regardless of the H₂ photodissociation, such clouds can start collapsing dynamically. It is frequently assumed that, even in primordial clouds that cool by the atomic cooling instead of the H₂ one, star formation occurs in the same way as in those with the H₂ cooling. However, it is far from evident.

Recall another role of hydrogen molecules in primordial star formation. The formation of protostars in primordial clouds with H₂ cooling has been investigated by many authors (e.g., Matsuda et al. 1969; Yoneyama 1972; Carlberg 1981; Palla et al. 1983; Omukai & Nishi 1998). It is known that those clouds cool by H₂ rovibrational line emission (for number density $n \lesssim 10^{14}$ cm⁻³), H₂ collision-induced emission (for $10^{14} \lesssim n \lesssim 10^{16}$ cm⁻³), and the H₂ dissociation (for $n \lesssim 10^{20}$ cm⁻³). Eventually, a very small protostar ($\sim 10^{-3}M_{\odot}$) forms at the center when $n \simeq 10^{22}$ cm⁻³.

On the other hand, we know little about the later evolution of clouds that start collapsing via atomic cooling. It is still unclear under what condition H₂ eventually forms, or whether it plays some role as a coolant in such clouds. It is also not known how small a Jeans mass is reached through atomic cooling alone. If this value falls well beyond the mass of normal stars (for example if it corresponds to the size of super massive stars or very massive objects), we must conclude that normal stars does not form only by atomic cooling. The aim of this paper is to answer these questions.

¹Some authors use the term “soft-UV”, instead of “far-UV”, for radiation whose energy is below the Lyman limit.

In this paper, we study the thermal and chemical evolution of primordial clouds irradiated with FUV radiation. Thereby, we demonstrate that the Jeans mass inside the clouds is reduced to much less than a solar mass even in the absence of molecular cooling. This implies that low-mass primordial star formation is possible even without H_2 if fragmentation of the clouds occurs at sufficiently high density.

The outline of this paper is as follows. In §2, the method of our calculations is described. In §3, results of our calculations are presented. Finally, our work is summarized and its implications sketched briefly in §4.

2. Model

We consider spherical clouds of hydrogen-helium gas irradiated with FUV radiation. Specifically, we investigate the cases of two FUV spectra in this paper: type *a*, the power-law radiation

$$J_{\text{UV}}(\nu) = J_{21} \times 10^{-21} (\nu/\nu_{\text{th}})^{-1} \text{ (erg s}^{-1} \text{ cm}^{-2} \text{ str}^{-1} \text{ Hz}^{-1}) \quad (\nu < \nu_{\text{th}}), \quad (1)$$

and type *b*, the diluted thermal radiation of 10^4 K

$$J_{\text{UV}}(\nu) = J_{21} \times 10^{-21} \frac{B(\nu; 10^4\text{K})}{B(\nu_{\text{th}}; 10^4\text{K})} \text{ (erg s}^{-1} \text{ cm}^{-2} \text{ str}^{-1} \text{ Hz}^{-1}) \quad (\nu < \nu_{\text{th}}), \quad (2)$$

where ν_{th} is the Lyman limit frequency. In both cases, $J_{\text{UV}}(\nu) = 0$ beyond the Lyman limit. We neglect the so-called sawtooth modulation due to the absorption of Lyman series photons by the intergalactic matter (e.g., Haiman et al. 1997), for simplicity. This suffices for our simple analysis, which is valid only in order-of-magnitude estimates. We also include the cosmic microwave background radiation (CMBR), although it has little influence on the matter at those low redshifts. The spectra of FUV radiation are shown in Figure 1 for $J_{21} = 1$ along with the CMBR at $z = 30$. Note that, for the same value of intensity at the Lyman limit, the number of photons above the threshold of H^- photodissociation is larger for type *b* spectra than for type *a* spectra. Consequently, the photodissociation rate of H^- is about 250 times larger for the $T = 10^4$ K thermal type radiation (type *b*) than for the power-law type (type *a*) with the same value of J_{21} . Similarly, the photodissociation rate of H_2 is about 3 times larger for the type *b* spectrum.

We take the maximum expansion of an overdensity as the initial condition of the calculation. Assuming the redshift of that epoch $z_{\text{m}} \simeq 30$, we take the number density of hydrogen nuclei $n = (\Omega_{\text{b}}/\Omega_0)[\rho/(1+4y_{\text{He}})m_{\text{H}}]$, ionization degree $y(e)$, and matter temperature T_{m} at the maximum expansion epoch as $n = 8.9 \times 10^{-2} \text{ cm}^{-3}$, $T = 39\text{K}$, $y(e) = 2.0 \times 10^{-4}$, respectively. We neglect the initial molecular abundance and assume $y(\text{H}_2) = 0$. Here y_{He} is the concentration of helium nuclei, and m_{H} is the mass of a hydrogen nucleus. Note that the concentration of He is defined by $y_{\text{He}} = n_{\text{He}}/n$, where n and n_{He} are the number density of hydrogen nuclei and helium nuclei, respectively. Simultaneously, we write for each atomic, molecular, or ionic species, $y(x) = n(x)/n$, where $n(x)$ is the number density of species x . Note $y(\text{H}_2) = 1/2$ for fully molecular gas. We set the

primordial helium abundance at $y_{\text{He}} = 0.0807$, which corresponds to the mass fraction $Y_{\text{p}} = 0.244$ (Izotov & Thuan 1998). The cosmological parameters are $\Omega_0 = 1$, $\Omega_{\text{b}} = 0.05$, and $h = 0.7$.

Any effect due to rotation or magnetic fields are neglected for simplicity. Then, the actual collapse is expected to proceed like the Penston-Larson similarity solution (Penston 1969; Larson 1969).² According to this solution, the cloud consists of two parts, that is, a central core region and an envelope. The central core region has a flat density distribution, whereas in the envelope, the density decreases outward as $\propto r^{-2}$. The size of the central flat region is roughly given by the local Jeans length $\lambda_{\text{J}} = \pi c_{\text{s}}/\sqrt{G\rho}$, where c_{s} and ρ are the sound speed and total density in the core, respectively. In this paper, we take the radius of the central region as $R_{\text{c}} = \lambda_{\text{J}}/2$. The collapse in the core proceeds approximately at the free-fall rate. In this paper, we focus on the evolution in the central region. In particular, we calculate the the temperature and chemical composition of the collapsing core as a function of the central density.

The cloud consists of two components, namely, baryon and dark matter. We assume that the dynamics of the baryonic component is described by the relation

$$\frac{d\rho_{\text{b}}}{dt} = \frac{\rho_{\text{b}}}{t_{\text{ff}}}, \quad (3)$$

where ρ_{b} is the baryonic density in the central region and the free-fall time is

$$t_{\text{ff}} \equiv \sqrt{\frac{3\pi}{32G\rho}}. \quad (4)$$

The dynamics of the dark matter is described by the relation for the top-hat overdensity,

$$\rho = \frac{9\pi^2}{2} \left(\frac{1+z_{\text{m}}}{1-\cos\theta} \right)^3 \Omega_0 \rho_{\text{c}}, \quad (5)$$

up to the virialization, where the maximum expansion redshift $z_{\text{m}} = 30$, and the parameter θ is related to z by the relation

$$1+z = (1+z_{\text{m}}) \left(\frac{\theta - \sin\theta}{\pi} \right)^{2/3} \quad (6)$$

(e.g., Padmanabhan 1993). We also use the usual age-redshift relation for the matter dominant universe, $t = 3.1 \times 10^{17}(\text{s})h^{-1}\Omega_0^{-1/2}(1+z)^{-3/2}$. After the virialization of dark matter, i.e., when the density reaches to the virial density $\rho_{\text{DM,vir}} = 8\rho_{\text{DM}}(z_{\text{m}})$, we keep $\rho_{\text{DM}} = \rho_{\text{DM,vir}}$.

The thermal evolution is followed by solving the energy equation

$$\frac{de}{dt} = -p \frac{d}{dt} \left(\frac{1}{\rho_{\text{b}}} \right) - \frac{\Lambda_{\text{net}}}{\rho_{\text{b}}}, \quad (7)$$

²Although the original Penston-Larson similarity solution is limited to the isothermal collapse, Yahil (1983) extended this solution for general polytropic equations of state.

where

$$e = \frac{1}{\gamma_{\text{ad}} - 1} \frac{kT}{\mu m_{\text{H}}} \quad (8)$$

is the internal energy per unit mass of baryon,

$$p = \frac{\rho_{\text{b}} kT}{\mu m_{\text{H}}} \quad (9)$$

is the pressure for an ideal gas, γ_{ad} is the adiabatic exponent, T is the temperature, μ is the mean molecular weight, m_{H} is the mass of a hydrogen nucleus, and Λ_{net} is the net cooling rate per unit volume. The net cooling rate Λ_{net} consists of contributions from radiative cooling or heating by atomic hydrogen lines Λ_{H} ; by rovibrational lines of molecular hydrogen, Λ_{H_2} ; by continuum, Λ_{cont} ; and by the Compton coupling with the radiation, Λ_{Compt} (the Compton cooling is unimportant in those low redshifts although it is included in our calculation) and from heating and cooling associated with chemical reactions, Λ_{chem} :

$$\Lambda_{\text{net}} = \Lambda_{\text{H}} + \Lambda_{\text{H}_2} + \Lambda_{\text{cont}} + \Lambda_{\text{Compt}} + \Lambda_{\text{chem}}. \quad (10)$$

The continuum processes included are listed in Table 1. The details of these processes are described in Appendix B. Since we are focusing on the evolution of the central region, whose radius $R_{\text{c}} = \lambda_{\text{J}}/2$, then we evaluate the optical depth τ_{ν} by

$$\tau_{\nu} = \kappa_{\nu} R_{\text{c}} = \kappa_{\nu} \left(\frac{\lambda_{\text{J}}}{2} \right). \quad (11)$$

Time-dependent nonequilibrium chemical reactions are solved for the following nine species: H, H₂, e, H⁺, H₂⁺, H⁻, He, He⁺, and He⁺⁺. Chemical reactions included are listed in Table 2.

3. Results

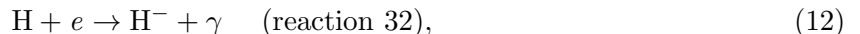
In this section, we present our numerical results. Figures 2 and 3 display the temperature evolution for collapsing primordial clouds irradiated with (1) the power-law type and (2) diluted black body of 10⁴ K type FUV radiation, respectively. As mentioned in §2, the photodissociation rate coefficients of both H⁻ and H₂ are larger for type *b* spectrum than for the type *a* with the same value of J_{21} . Consequently, FUV radiation of type *b* has the larger influence on the evolution of the clouds than type *a* with the same value of J_{21} . We discuss effects of different spectral types and scaling relations between them in Appendix A. Except for those scalings of J_{21} , the evolutionary trajectories change in similar ways with an increase of the UV intensity in both cases. Hence, we describe only the evolutionary features of the clouds irradiated with type *a* radiation in detail here.

The evolutionary trajectories for the clouds with $J_{21} \geq 10^5$ are identical to each other. As is obvious from Figure 2, the thermal evolution at high densities (say, $n \gtrsim 10^7 \text{cm}^{-3}$) is completely different between clouds with $J_{21} \leq 10^4$ and those with $J_{21} \geq 10^5$. This is because the clouds

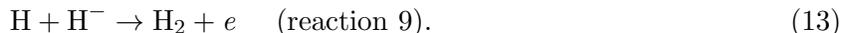
irradiated by the FUV radiation with $J_{21} \geq 10^5$ cannot form sufficient H_2 , so they cool only by atomic cooling. The temperature of such clouds is higher than that of clouds with $J_{21} \leq 10^4$, which can form enough H_2 to cool eventually. Toward higher densities, these two groups of trajectories in Figure 1 converge respectively to two different limiting tracks. We call the higher temperature one the “atomic cooling track”, and the other the “molecular cooling track”. This nomenclature comes from the fact that clouds evolving along the former track remain atomic, while those following the latter eventually become fully molecular. We should note that the Jeans masses inside the clouds ultimately fall below $0.1M_\odot$ for both tracks.

Figure 4 shows the fractional abundances of hydrogen molecules (Fig.4a) and electrons (Fig.4b) for the clouds irradiated with type *a* radiation. The separate heating and cooling rates per unit mass for those clouds are illustrated in the panels of Figure 5 for $J_{21} = 0$ (Fig.5a), 10^4 (Fig.5b) and 10^5 (Fig.5c).

We review their evolutionary features starting from the case of $J_{21} = 0$. In this case, the collapse proceeds along the well-known molecular cooling track (e.g., Palla et al. 1983). At the beginning, the temperature rises adiabatically owing to the compression and the initial lack of coolant. If the total mass of the cloud is less than the maximum Jeans mass attained at the end of this adiabatic phase, the contraction stops at the time when the cloud mass becomes equal to the Jeans mass. We assume here that the total mass of the cloud is larger than the maximum Jeans mass. At low densities (i.e., $n \lesssim 10^8 \text{cm}^{-3}$), H_2 is formed mainly through the H^- channel:



and then



Increased temperature and density causes an increase of both the H_2 formation rate and the H_2 cooling function. Consequently, a sufficient amount of H_2 to cool within a free-fall time is formed, and the temperature then drops. A detailed discussion of when the efficient H_2 cooling begins is presented in Appendix A. Owing to the H_2 cooling, the temperature is kept as low as a few hundred K in the cloud (see Fig.2 and Fig.5a). When the density reaches about 10^8cm^{-3} , the three-body reaction



becomes efficient (Palla et al. 1983). In consequence of this highly productive H_2 formation, hydrogen becomes fully molecular (see Fig.4 a). At the same time, the cloud becomes optically thick to a few H_2 lines at $n \simeq 10^{11} \text{cm}^{-3}$. However, the cooling remains efficient enough to induce dynamical collapse (i.e., The ratio of specific heat $\Gamma \equiv d \log p / d \log \rho < 4/3$) because there are still enough optically thin lines. When the central number density reaches about 10^{14}cm^{-3} , H_2 collision-induced emission begins to dominate the cooling (see Fig.5a). The cloud becomes optically thick to this continuum at $\sim 10^{16} \text{cm}^{-3}$. Thereafter, the radiative cooling rate drops rapidly. Simultaneously, H_2 dissociation begins, because the temperature is already near the value needed for dissociation. The H_2 dissociation prevents the temperature from rising rapidly until the number density reaches

about 10^{20}cm^{-3} . The minimum Jeans mass of $1.5 \times 10^{-3}M_{\odot}$ is reached shortly after that. When most of the hydrogen molecules are dissociated, the collapse becomes approximately adiabatic. According to Omukai & Nishi (1998), after a little further contraction, a small hydrostatic core (about a few $10^{-3}M_{\odot}$), or protostar, forms at $n \simeq 10^{22}\text{cm}^{-3}$, $T \simeq 3 \times 10^4\text{K}$.

As seen in Figure 2, if the intensity of FUV radiation increases, the density and temperature at the time when efficient H_2 cooling begins also increases (see Appendix A for further discussion). After H_2 cooling becomes effective, the trajectories of those clouds soon converge to the evolutionary track for $J_{\text{UV}}(\nu) = 0$.

An interesting example is when the intensity is as high as $J_{21} \simeq 10^4$. In this case, the temperature rises almost adiabatically up to about 8000K without enough H_2 formation. At that point, $\text{Ly}\alpha$ line emission of atomic hydrogen begins to work as an efficient cooling agent (see Fig.5b). After the cloud collapses isothermally at $T \simeq 8000\text{K}$ over an order of magnitude in density owing to this coolant, sufficient hydrogen molecules form as a result of the increased density. Thereafter, the trajectory converges rapidly to the molecular cooling track in the same way as those with weaker radiation (see Fig.2).

When the intensity of FUV radiation is increased more, i.e., $J_{21} \gtrsim 10^5$, the thermal evolution becomes completely different from those with lower intensities (see Fig.2). The adiabatic rise of temperature continues until $\text{Ly}\alpha$ cooling becomes effective at about 8000K.³ While the cloud collapses nearly isothermally at about 8000K owing to $\text{Ly}\alpha$ line cooling, the central density reaches the critical density⁴ $n_{\text{cr}} \simeq 10^4\text{cm}^{-3}$ of hydrogen molecules before a amount of H_2 sufficient to cool within a free-fall time forms. At higher densities, $n \gtrsim n_{\text{cr}}$, enough H_2 never forms, for the following two reasons. First, the H_2 fraction decreases; the collisional dissociation rate coefficient increases because, at $n \gtrsim n_{\text{cr}}$, high vibrational levels, at which dissociation occurs easily, are populated by more hydrogen molecules than at lower density. Second, the amount of H_2 needed for efficient cooling increases; note that the cooling rate per unit volume $\Lambda_{\text{H}_2} \propto n^2$ for $n \lesssim n_{\text{cr}}$, while $\Lambda_{\text{H}_2} \propto n$ for $n \gtrsim n_{\text{cr}}$. (see Appendix A for further discussion). Consequently, the cloud never joins to the molecular cooling track. Instead, it continues to cool by $\text{Ly}\alpha$ line emission until the density reaches about 10^6cm^{-3} , where collisional de-excitation from the $2p$ state begins to dominate the $\text{Ly}\alpha$ emission as a result of the small escape probability (i.e., $\beta_{\text{esc},21}A_{21} \simeq C_{21}$). The subsequent major cooling process is two-photon emission of atomic hydrogen from the $2s$ state. This works effectively in the density range $10^6\text{cm}^{-3} \lesssim n \lesssim 10^7\text{cm}^{-3}$. Next, the cloud cools by the free-bound emission of H^- over nearly ten orders of magnitude in density, until the number density reaches 10^{16}cm^{-3} (see Fig.5 c). The mechanism of H^- free-bound emission cooling is as follows. As a first

³The initial slight rise of ionization degree seen in Figure 4b is caused by photoionization from the first excited level, which is populated by more atoms than the local thermodynamic equilibrium (LTE) value as a result of absorption of irradiated $\text{Ly}\alpha$ photons. This effect has little influence on the later evolution.

⁴The critical density is the density above which the rovibrational levels of H_2 are populated, according to the LTE law.

step, radiative association of H and e ;



occurs and a photon is emitted. This H^- is used to form H_2 (reaction 9), which will be collisionally dissociated by reaction 15. As a result, there is net cooling by the photon emitted in reaction 32.⁵ In the course of the dynamical collapse induced by H^- free-bound emission, the temperature falls gradually from 7000K (at $n \simeq 10^6 \text{cm}^{-3}$) to 3000K (at $n \simeq 10^{16} \text{cm}^{-3}$; see Fig. 2). At the central density, $\sim 10^{16} \text{cm}^{-3}$, the cloud becomes optically thick to both H^- bound-free absorption and Rayleigh scattering of atomic hydrogen. At the number density $\simeq 10^{17} \text{cm}^{-3}$, the H ionization begins (see Fig. 4 b). As a result, the temperature rise slows down up to $n \simeq 10^{19} \text{cm}^{-3}$. At $n = 10^{20} \text{cm}^{-3}$, where 60 % of the gas is ionized, the minimum Jeans mass $M_{\text{J,min}} = 0.03M_{\odot}$ is reached. Thereafter, the temperature continues to rise almost adiabatically. We expect that a protostar on the order of $M_{\text{J,min}}$ is formed after a little further adiabatic contraction. Although the minimum Jeans mass of the atomic cooling clouds is 20 times larger than that of the H_2 cooling clouds, it is still much less than the mass of usual stars.

4. Summary and Discussion

We have investigated the thermal and chemical evolution of primordial clouds irradiated with FUV radiation. When intensity of the irradiating FUV radiation exceeds some critical value [$J_{21} \simeq 10^5$ for $J_{\text{UV}}(\nu) \propto \nu^{-1}$ ($h\nu < 13.6\text{eV}$)], sufficient molecular hydrogen to be important for cooling is never formed in those clouds because of the photodissociation and blocking of the formation channel. Nonetheless, sufficiently massive clouds can start dynamical collapse by atomic line cooling even without H_2 . Those clouds continue to collapse almost isothermally at several thousand K along the “atomic cooling track” in the density-temperature plane. That dynamical collapse is induced by successive cooling by $\text{Ly}\alpha$ emission, two-photon emission, and H^- free-bound emission. The minimum Jeans mass eventually reduces to about $0.03M_{\odot}$ for those clouds. On the other hand, clouds irradiated with less intense FUV radiation collapse dynamically by the H_2 cooling. The minimum Jeans mass of such clouds is about $1.5 \times 10^{-3}M_{\odot}$.

Although in this paper we limited our application to the protostellar collapse under an FUV background, we expect that the primordial protostellar collapse without H_2 also occurs in other situations. Recently, Susa & Kitayama (2000) investigated the collapse of primordial clouds irradiated with ionizing UV background $J_{\text{UV}}(\nu) = J_{21} \times 10^{-21}(\nu/\nu_{\text{th}})^{-1}$ ($\text{erg s}^{-1}\text{cm}^{-2}\text{str}^{-1}\text{Hz}^{-1}$). They pointed out that H_2 formation is suppressed for $J_{21} > 3.6 \times 10^4$ owing to blocking of the H_2 formation channel by H^- photodissociation. Although they did not study the later evolution, we guess that the clouds continue collapsing along our atomic cooling track. Carlberg (1981) also

⁵Formed H^- is photodissociated at low densities, that is, $n < k_{31}/k_9 = 0.1\alpha J_{21}$, where α is a constant defined in Appendix A, and is 8 for the type a (2×10^3 for type b , respectively) spectrum. In this case, there is no net cooling.

considered the thermal evolution of collapsing primordial clouds without external radiation, but he did not include the three-body process of H_2 formation. For this reason, in his calculation, molecular hydrogen dissociates at $n \simeq 10^{11} \text{cm}^{-3}$. After that, the evolutionary path of his cloud follows approximately our atomic cooling track (see Fig. 2 of Carlberg 1981). This fact supports our speculation that the clouds that do not cool by H_2 collapse along the atomic cooling track.

Next, we discuss the feasibility of the collapse along the atomic cooling track in the cosmological reionization. The UV intensity needed to reionize the universe at z_{reion} , i.e., 1 ionizing photon per a hydrogen nucleus, is

$$J_{\text{reion}} = \frac{hc\Omega_b\rho_{\text{cr}}(1+z_{\text{reion}})^3}{4\pi(1+4y_{\text{He}})m_{\text{H}}} = 3 \times 10^{-21} \left(\frac{1+z_{\text{reion}}}{10}\right)^3 \text{ (erg s}^{-1} \text{ cm}^{-2} \text{ str}^{-1} \text{ Hz}^{-1}) \quad (16)$$

at the Lyman limit for $J(\nu) \propto \nu^{-1}$ and the assumed cosmological parameters. Thus, the condition that the clouds collapse along the atomic cooling track, $J_{21} \gtrsim 10^5$ for $J_{\text{UV}}(\nu) \propto \nu^{-1}$, seems to be rarely met in practice, except in the immediate vicinity of UV sources.

Finally, we discuss the mass of formed stars. Although the minimum Jeans mass is less than $0.1 M_{\odot}$, this corresponds not to the final mass of formed stars, but rather to the initial mass of the protostar, which has no direct relation with the former. When a small hydrostatic core, namely protostar, forms at the center of a collapsing protostellar cloud, an enormous amount of gravitationally unstable gas still surrounds the protostar. Thereafter, the protostar grows in mass by accreting the ambient matter. Consequently, the final mass of stars is determined by the subsequent accretion onto the protostar. Stahler, Shu, & Taam (1980) argued that a rough estimate of the protostellar mass accretion rate \dot{M} can be obtained from the relation $\dot{M} \sim c_s^3/G$, where c_s is the isothermal sound speed in the protostellar cloud. From this relation, the mass accretion rate is higher for protostars formed by atomic cooling than for those formed by molecular cooling because of the higher temperature of the protostellar cloud. Suppose that the accretion is halted by some stellar activity, e.g., radiation force, bipolar flow, etc. In this case, the higher accretion rate probably results in the later halting and higher mass of formed stars (e.g., Wolfire & Cassinelli 1987).

In contrast, from the viewpoint of fragmentation, the masses of primordial stars formed by atomic cooling alone could be smaller than those formed by molecular cooling. The fragmentation is possible in principle as long as the temperature decreases toward higher density, while it does not occur after the isothermality of the cloud breaks down and the temperature begins to rise (Inutsuka & Miyama 1997; Masunaga & Inutsuka 1999). From Figures 2 and 3, the final fragmentation occurs at about $n \simeq 10^{16} \text{cm}^{-3}$ for clouds collapsing along the atomic cooling track. On the other hand, it seems difficult for molecular cooling clouds to fragment at $n \gtrsim 10^3 \text{cm}^{-3}$. The masses of fragments, which is about the Jeans mass at that time, are about $0.1M_{\odot}$ for the atomic-cooling clouds, and 10^4M_{\odot} for the molecular-cooling clouds. If this is the case and the whole material contained in a fragment is converted into a single star, very massive stars form from a molecular-cooling cloud, and red dwarfs form as a result of atomic cooling. However, it should be noted that the fragmentation

and thermal evolution depend strongly on each other and also on the geometry of the clouds. In fact, Uehara et al. (1996) concluded that the minimum mass of fragments is on the order of a solar mass, which is essentially the Chandrasekhar mass, by studying thermal evolution of filamentary primordial clouds that collapse by molecular cooling. Later, improved simulations by Nakamura & Umemura (1998) confirmed Uehara et al.(1996)’s result. The discrepancy between our mass of fragments ($\sim 10^4 M_\odot$) and theirs ($\sim 1 M_\odot$) results from the difference of the assumed geometry of the clouds; we have assumed spherical clouds in studying the thermal evolution, while their clouds are filamentary. For filamentary clouds, the gravitational contraction is slower and compressional heating rate is lower than for spherical ones. Hence, for the filamentary cloud the isothermality breaks down at higher density, where the Jeans mass is smaller. To fully address the complexity arising from the cloud geometry, two-dimensional or three-dimensional calculations are needed. Furthermore, there are other uncertainties relating to the evolution of the fragments, for example, mass accretion onto the fragments, merger between them, feedback from neighboring formed stars, etc. (e.g., Bromm et al. 1999). It seems premature to draw conclusions here about these issues.

I would like to thank Shu-ichiro Inutsuka, Ryoichi Nishi, Humitaka Sato, Toru Tsuribe for crucial suggestions and discussions, and Phil Stancil for providing the data of the H_2^+ photodissociation cross section. I also acknowledge the referee for improving the manuscript. This work is supported in part by Research Fellowships of the Japan Society for the Promotion of Science for Young Scientists, grant 4287.

A. Conditions for H₂ Cooling

In this section, we discuss key processes determining the amount of the molecular hydrogen forming under FUV radiation. In particular, we delineate the condition for sufficient H₂ for cooling to form.

The H₂ fraction $y(\text{H}_2)$ necessary to cool within a free-fall time is given by

$$y_{\text{cool}}(\text{H}_2) = \frac{(3/2)k_{\text{B}}T}{nL_{\text{H}_2}t_{\text{ff}}}, \quad (\text{A1})$$

where $L_{\text{H}_2}(\text{erg s}^{-1} \text{ cm}^3) = \Lambda_{\text{H}_2}/n(\text{H})n(\text{H}_2)$ is the H₂ cooling function and we assume $n(\text{H}) \simeq n$. When the actual H₂ fraction $y(\text{H}_2)$ reaches $y_{\text{cool}}(\text{H}_2)$, the temperature drops abruptly as seen in Figure 2 and 3.

Next, we discuss how much H₂ forms during the collapse. The H₂ abundance is bounded by the following three values;

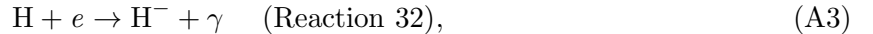
- (1) the amount of H₂ that is able to form within a free-fall time, $y_{\text{form}}(\text{H}_2)$,
- (2) the chemical equilibrium value between H₂ formation and photodissociation, $y_{\text{pd}}(\text{H}_2)$,
- (3) the chemical equilibrium value between H₂ formation and collisional dissociation, $y_{\text{cd}}(\text{H}_2)$.

In practice, the smallest among these three values is realized;

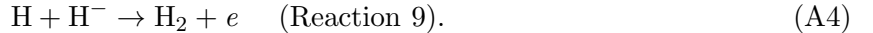
$$y(\text{H}_2) = \min[y_{\text{form}}(\text{H}_2), y_{\text{pd}}(\text{H}_2), y_{\text{cd}}(\text{H}_2)]. \quad (\text{A2})$$

In the following, we examine the values of $y_{\text{form}}(\text{H}_2)$, $y_{\text{pd}}(\text{H}_2)$, and $y_{\text{cd}}(\text{H}_2)$ in this order.

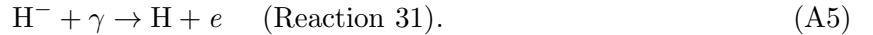
First, we find the formation time limited value $y_{\text{form}}(\text{H}_2)$. H₂ formation occurs mainly through the H[−] channel:



followed by



In the above chain, not all of H[−] formed are used in H₂ formation. Instead, some of H[−] are photodissociated via Reaction 31;



The photodissociation rate coefficient of H[−], k_{31} , depends on the spectrum of radiation. Here, we introduce a parameter α , defined by

$$k_{31} = \alpha \kappa_{31} J_{21}, \quad (\text{A6})$$

where $\kappa_{31} = 1 \times 10^{-10}$ is the value of k_{31} under $J_{\text{UV}}(\nu) = 10^{-21} = \text{const.}$ (for $\nu < \nu_{\text{th}}$). The parameter α characterizing the radiation spectrum above H[−] photodissociation threshold (0.755

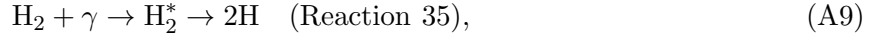
eV) is 8 for the power-law type spectrum (type *a* in the text), 2×10^3 for the diluted thermal type spectrum (type *b*). The rates of the competing reactions 9 and 31 determine the branching ratio of H^- to be used in H_2 formation, which is $k_9 n / (k_9 n + k_{31})$. Then, by defining the effective H_2 formation rate coefficient

$$k_{\text{form}} = k_{32} \frac{k_9 n}{k_9 n + k_{31}}, \quad (\text{A7})$$

the H_2 formation rate can be written as $k_{\text{form}} n(e)n(\text{H})$. Using k_{form} above, we obtain the H_2 fraction that can form within a free-fall time

$$y_{\text{form}}(\text{H}_2) = k_{\text{form}} y(e) n t_{\text{ff}}. \quad (\text{A8})$$

Second, we find the photodissociation limited value $y_{\text{pd}}(\text{H}_2)$. The photodissociation occurs via



whose reaction coefficient is

$$k_{\text{pd}} \equiv k_{35} = 10^9 J(h\nu = 12.4\text{eV}) f_{\text{sh}} = 10^{-12} \beta J_{21} f_{\text{sh}}. \quad (\text{A10})$$

Here, we have introduced a parameter β that represents the relative strength of radiation intensity at the average LW band frequency (12.4 eV) to that at the Lyman limit (13.6 eV). The shielding factor f_{sh} is given by (Draine & Bertoldi 1996)

$$f_{\text{sh}} = \min \left[1, (N_{\text{H}_2} / 10^{14} \text{cm}^{-2})^{-3/4} \right]. \quad (\text{A11})$$

The equilibrium value between the H_2 formation and photodissociation is

$$y_{\text{pd}}(\text{H}_2) = \frac{k_{\text{form}}}{k_{\text{pd}}} y(e) n. \quad (\text{A12})$$

If $N_{\text{H}_2} > 10^{14} \text{cm}^{-2}$, the coefficient k_{pd} , and then the right hand side of equation (A12), involves $y(\text{H}_2)$ itself. Denoting $k_{\text{pd}} = a_{\text{pd}} y(\text{H}_2)^{-3/4}$, where $a_{\text{pd}} \equiv 7 \times 10^{-18} T_3^{-3/8} n^{-3/8} \beta J_{21}$, we obtain

$$y_{\text{pd}}(\text{H}_2) = \left(\frac{k_{\text{form}}}{a_{\text{pd}}} y(e) n \right)^4 \quad (N_{\text{H}_2} > 10^{14} \text{cm}^{-2}). \quad (\text{A13})$$

Combining expressions for cases with and without H_2 self-shielding, the photodissociation limited value of H_2 is

$$y_{\text{pd}}(\text{H}_2) = \max \left[\frac{k_{\text{form}}}{10^{-12} \beta J_{21}} y(e) n, \left(\frac{k_{\text{form}}}{a_{\text{pd}}} y(e) n \right)^4 \right]. \quad (\text{A14})$$

Note that the radiation intensity enters into the expression for $y_{\text{pd}}(\text{H}_2)$ only in the form of $\alpha \beta J_{21}^2$ in the low density range $n < k_{31}/k_9 \simeq 0.1 \alpha J_{21} \text{cm}^{-3}$.

Third, the collisional dissociation limited value $y_{\text{cd}}(\text{H}_2)$ can be obtained as follows. The dominant collisional dissociation process is collision with the atomic hydrogen:



Then, denoting $k_{\text{cd}} \equiv k_{15}$,

$$y_{\text{cd}}(\text{H}_2) = \frac{k_{\text{form}}}{k_{\text{cd}}} y(e). \quad (\text{A16})$$

This value $y_{\text{cd}}(\text{H}_2)$ becomes smaller when the density exceeds the critical density $n_{\text{cr}} \simeq 10^4 \text{cm}^{-3}$ owing to the collisional dissociation from high vibrational states.

Now, we examine when sufficient H_2 forms under FUV radiation in the case that the temperature rises adiabatically from the initial value. Figure 6 shows the H_2 fraction estimated by Equation (A2) in this case. Here, the temperature is given by $T = T_0(n/n_0)^{2/3}$, where the initial number density and temperature are $n_0 = 8.9 \times 10^{-2} \text{cm}^{-3}$, $T_0 = 39\text{K}$, and the ionization degree $y(e)$ is fixed to 10^{-4} .⁶ In Figure 6, each curve for $y(\text{H}_2)$ with fixed FUV intensity consists of four segments. From the lowest to highest temperature in this Figure, those segments correspond to $y_{\text{pd}}(\text{H}_2)$ without self-shielding (gradually increasing portion), $y_{\text{pd}}(\text{H}_2)$ with self-shielding (rapidly increasing portion), $y_{\text{form}}(\text{H}_2)$ (another gradually increasing portion), and $y_{\text{cd}}(\text{H}_2)$ (decreasing portion). As known from Figure 6, except for lowest intensities (in such a case, the evolution of the cloud is virtually unaffected by the presence of FUV radiation), the photodissociation limited value $y_{\text{pd}}(\text{H}_2)$ determines when the sufficient H_2 forms. The condition that molecular cooling becomes effective before atomic cooling does is that $y_{\text{pd}}(\text{H}_2) > y_{\text{cool}}(\text{H}_2)$ at $T = 8000 \text{K}$, which leads to

$$J_{21} < 4 \times 10^3 \left(\frac{x_4}{\alpha\beta} \right)^{1/2}, \quad (\text{A17})$$

where $x_4 \equiv y(e)/10^{-4}$ and we have used $k_{\text{form}} \simeq k_{32}k_9n/k_{31}$, and $k_{32} = 3.6 \times 10^{-15}$, $k_9 = 8.7 \times 10^{-10}$, $y_{\text{cool}}(\text{H}_2) = 10^{-6}$, and $n = 2.6 \times 10^2 \text{cm}^{-3}$ at 8000K. Also, since FUV intensity enters into $y_{\text{pd}}(\text{H}_2)$ in the form of $\alpha\beta J_{21}^2$, type *b* spectrum of $J_{21}^{(b)}$ has the same effect as type *a* spectrum of $\sqrt{\alpha\beta(b)/\alpha\beta(a)} \simeq 27$ times $J_{21}^{(b)}$ on the early evolution of the clouds.

As discusses in the text, the cloud irradiated by strong FUV radiation never forms sufficient H_2 for cooling if the intensity exceeds a certain critical value. Next, we discuss the physical reason where this value comes from. Here, we examine how much H_2 forms while the cloud collapses isothermally owing to $\text{Ly}\alpha$ cooling. The values of H_2 concentration $y(\text{H}_2)$ estimated by equation (A2) for $T = 8000\text{K}$ and $y(e) = 10^{-4}$ are shown in Figure 7.⁷ For a given value of FUV intensity, $y(\text{H}_2)$ is limited by $y_{\text{pd}}(\text{H}_2)$ (an almost vertical line) in the lower density range and by $y_{\text{cd}}(\text{H}_2)$ (a smooth curve) in the higher density range. The formation time limited value $y_{\text{form}}(\text{H}_2)$ does not appear in this Figure. On the other hand, $y_{\text{cool}}(\text{H}_2)$ decreases in the low density regime, reaches the minimum at $n \simeq n_{\text{cr}} \simeq 10^4 \text{cm}^{-3}$, and increase in higher densities. As seen in Figure 7, the H_2 fraction $y(\text{H}_2)$ has no chance to reach $y_{\text{cool}}(\text{H}_2)$ in $n \gtrsim n_{\text{cr}} \simeq 10^4 \text{cm}^{-3}$. This is because the H_2

⁶Here and through out this section, we assume the ionization degree is constant, namely, the recombination and/or ionization time scale is longer than the evolutionary timescale of the system (i.e., free-fall time) Although this is somewhat oversimplification, it suffices for clarifying key processes determining the H_2 fraction.

⁷Once the actual H_2 fraction exceeds $y_{\text{cool}}(\text{H}_2)$, the temperature of the cloud drops from $\sim 8000\text{K}$ as a result of the H_2 cooling. After that, the H_2 fraction shown in the Figure does not represent the actual value.

fraction $y(\text{H}_2)$ is limited by $y_{\text{cd}}(\text{H}_2)$, which becomes small in those densities owing to the enhanced collisional dissociation from high vibrational levels. Therefore, in order for the H_2 cooling to become efficient, $y(\text{H}_2)$ must reach $y_{\text{cool}}(\text{H}_2)$ at $n \lesssim n_{\text{cr}}$; both $y_{\text{cd}}(\text{H}_2)$ and $y_{\text{pd}}(\text{H}_2)$ must exceed $y_{\text{cool}}(\text{H}_2)$ at $n \lesssim n_{\text{cr}} \simeq 10^4 \text{cm}^{-3}$. As the condition on $y_{\text{cd}}(\text{H}_2)$, we take $\gamma y_{\text{cd}} > y_{\text{cd}}(J(\nu) = 0)$, where constant $\gamma \sim$ several, noting that $y_{\text{cd}}(\text{H}_2; J(\nu) = 0)$ is several times larger than $y_{\text{cool}}(\text{H}_2)$ at $n \lesssim n_{\text{cr}}$. This reduces to $\gamma k_9 n_{\text{cr}} > k_{31}$, or in another expression,

$$J_{21} < 4 \times 10^5 \alpha^{-1}, \quad (\text{A18})$$

where we have chosen $\gamma = 5$. The condition on $y_{\text{pd}}(\text{H}_2)$ leads to another constraint on J_{21} :

$$J_{21} < 1 \times 10^6 x_4 \beta^{-1}. \quad (\text{A19})$$

Here, we have used $y_{\text{cool}} \simeq 10^{-6}$, since the dependence of $y_{\text{pd}}(\text{H}_2)$ on n is so strong that the precise value of $y_{\text{cool}}(\text{H}_2)$ is not important. Also, $k_{\text{form}} = k_{32}$ has been used. Combining the conditions (A18) and (A19), the critical intensity J_{cr} above which the cloud never forms sufficient H_2 is

$$J_{\text{cr},21} = \min(4 \times 10^5 \alpha^{-1}, 1 \times 10^6 x_4 \beta^{-1}). \quad (\text{A20})$$

Substituting the parameters α and β into equation (A20), we see that the former constraint is more restrictive than the latter for both two types of radiation discussed in the text.

B. Radiative Processes

B.1. Atomic Hydrogen Lines and Two-photon Emission

We model an atomic hydrogen as a five level system. The radiative cooling rate due to atomic hydrogen lines per unit volume is given by

$$\Lambda_{\text{H lines}} = \sum_{ul} h\nu_{ul} \beta_{\text{esc},ul} A_{ul} n_u(\text{H}) [S_{\text{H}}(\nu_{ul}) - J_{\text{cont}}(\nu_{ul})] / S_{\text{H}}(\nu_{ul}), \quad (\text{B1})$$

where $n_u(\text{H})$ is the population density of atomic hydrogen in the upper energy level u , A_{ul} is the Einstein radiation probability for a spontaneous downward transition, $\beta_{\text{esc},ul}$ is the probability for a emitted line photon to escape without absorption, and $h\nu_{ul}$ is the energy difference between the upper level u and the lower level l , and $J_{\text{cont}}(\nu_{ul})$ is the mean intensity of overlapping continuum at the line frequency ν_{ul} . The source function $S_{\text{H}}(\nu_{ul})$ is given by

$$S_{\text{H}}(\nu_{ul}) = \frac{2h\nu_{ul}^3}{c^2} \left(\frac{g_u n_l(\text{H})}{g_l n_u(\text{H})} - 1 \right)^{-1}. \quad (\text{B2})$$

The cooling rate due to the two photon emission is

$$\Lambda_{2\text{ph}} = h\nu_{21} \beta_{\text{esc},2\text{ph}} \Lambda_{21} n_2(\text{H}), \quad (\text{B3})$$

where Λ_{21} is the spontaneous downward transition probability by the two-photon emission. The escape probability $\beta_{\text{esc},2\text{ph}} = \exp(-\tau_a)$, where τ_a is the absorption optical depth owing to other continuum processes (a1-a7 in Table 1; See §B.3). We take only account of absorption by other continuum processes, since our clouds do not become optically thick to the two-photon continuum.

Relative population of each energy level is obtained from a solution of the equations of the detailed balance between levels (e.g., de Jong, Dalgarno, & Boland 1980; Tielens & Hollenbach 1985)

$$n_i(\text{H}) \sum_{j \neq i}^n R_{ij} = \sum_{j \neq i}^n n_i(\text{H}) R_{ji}, \quad (\text{B4})$$

where n is the total number of transitions included. The transition rate R_{ij} from level i to level j is given by

$$R_{ij} = \begin{cases} (A_{ij}\beta_{\text{esc},ij} + \Lambda_{ij}\beta_{\text{esc},2\text{ph}})(1 + Q_{ij}) + C_{ij} & \text{for } i > j \\ (g_j/g_i)(A_{ji}\beta_{\text{esc},ij} + \Lambda_{ji}\beta_{\text{esc},2\text{ph}})Q_{ji} + C_{ij} & \text{for } i < j, \end{cases} \quad (\text{B5})$$

where C_{ij} is the collisional transition rate, and

$$Q_{ij} = \frac{c^2}{2h\nu_{ij}^3} J_{\text{cont}}(\nu_{ij}). \quad (\text{B6})$$

The relative population within the first excited states (i.e., $2p$ and $2s$ states) is obtained from the statistical equilibrium (Spitzer & Greenstein 1951),

$$\frac{n_{2s}}{n_{2p}} = \frac{g_{2s}}{g_{2p}} \left(\frac{C_{2s2p}}{C_{2s2p} + A_{2s1s}} \right), \quad (\text{B7})$$

where the statistical weight $g_{2s} = 2$, and $g_{2p} = 6$, the radiative transition rate by two photon emission $A_{2s1s} = 8.23(\text{s}^{-1})$, and the collisional transition rate between the levels

$$C_{2s2p} = 6.21 \times 10^{-4} T^{-1/2} \ln(5.7T) \left[1 + \frac{0.78}{\ln(5.7T)} \right] n(\text{e})(\text{s}^{-1}). \quad (\text{B8})$$

Using n_{2p} obtained above, we may write

$$A_{21} = \frac{n_{2p}}{n_2} A_{2p1s} \quad (\text{B9})$$

where $A_{2p1s} = 6.27 \times 10^8 (\text{s}^{-1})$.

We assume LTE within levels of the same principal quantum number for $n \geq 3$. Averaged over angular momentum quantum numbers, $A_{31} = 5.575 \times 10^7$, $A_{41} = 1.278 \times 10^7$, $A_{51} = 4.125 \times 10^6$, $A_{32} = 4.410 \times 10^7$, $A_{42} = 8.419 \times 10^6$, $A_{52} = 2.530 \times 10^6$, $A_{43} = 8.986 \times 10^6$, $A_{53} = 2.201 \times 10^6$, $A_{54} = 2.699 \times 10^6$ (Janev et al. 1987).

Likewise, we use the two-photon emission rate $\Lambda_{21} = (n_{2s}/n_2)A_{2s1s}$ and $\Lambda_{ul} = 0$ for other transitions.

The collisional de-excitation rate is given by

$$C_{ul} = \gamma_{ul}(e)n(e) + \gamma_{ul}(H)n(H), \quad (\text{B10})$$

where the collisional de-excitation rate coefficients $\gamma_{ul}(e)$ for collisions with electron and $\gamma_{ul}(H)$ for those with atomic hydrogen are given below.

The collisional de-excitation rate coefficients for collisions with electron is given by

$$\gamma_{ul}(e) = 10^{-8} \left(\frac{l^2}{u^2 - l^2} \right)^{3/2} \frac{l^4}{u^2} \alpha_{lu} \frac{\sqrt{\beta(\beta+1)}}{\beta + \chi_{lu}}, \quad \beta = \frac{h(\nu_l - \nu_u)}{kT}, \quad (\text{B11})$$

(Sobelman et al. 1981), where $\alpha_{12} = 24, \alpha_{13} = 22, \alpha_{14} = 22, \alpha_{15} = 21, \alpha_{23} = 67, \alpha_{24} = 58, \alpha_{25} = 56, \alpha_{34} = 124, \alpha_{35} = 101, \alpha_{45} = 185$ and $\chi_{12} = 0.28, \chi_{13} = 0.37, \chi_{14} = 0.39, \chi_{15} = 0.41, \chi_{23} = 0.30, \chi_{24} = 0.45, \chi_{25} = 0.52, \chi_{34} = 0.26, \chi_{35} = 0.42, \chi_{45} = 0.21$. For collisions with atomic hydrogen (Drawin 1969),

$$\gamma_{ul}(H) = 7.86 \times 10^{-15} \left(\frac{l}{u} \right)^2 (1/l^2 - 1/u^2)^{-2} f_{lu} T^{1/2} \frac{1 + 1.27 \times 10^{-5} (1/l^2 - 1/u^2)^{-1} T}{1 + 4.76 \times 10^{-17} (1/l^2 - 1/u^2)^{-2} T^2}, \quad (\text{B12})$$

where $f_{12} = 0.4162, f_{13} = 7.910 \times 10^{-2}, f_{14} = 2.899 \times 10^{-2}, f_{15} = 1.394 \times 10^{-2}, f_{23} = 0.6407, f_{24} = 0.1193, f_{25} = 4.467 \times 10^{-2}, f_{34} = 0.8421, f_{35} = 0.1506, f_{45} = 1.038$.

The collisional excitation rate can be obtained from the detailed balance:

$$C_{lu} = C_{ul}(g_u/g_l) \exp(-h\nu_{ul}/kT). \quad (\text{B13})$$

Taking into account the collisional de-excitation of line photons and absorption due to the overlapping continuum, we may write the escape probability as

$$\beta_{\text{esc},ul} = \frac{p_{ul}^{N_{\text{esc}}}}{1 + N_{\text{esc}}} \exp(-\tau_a), \quad (\text{B14})$$

where p_{ul} is the probability for an absorbed line photon to re-emerge as an original line photon with neither collisional de-excitation nor two photon continuum emission, and N_{esc} is the number of scattering that an average photon experiences before escape. The re-emergence probability can be written as

$$p_{ul} = \frac{A_{ul}}{A_{ul} + C_{ul} + \Lambda_{ul}}. \quad (\text{B15})$$

The average number of scattering for Ly α line in large optical depth τ_{21} limit is given by (Bonilha et al. 1979)

$$N_{\text{esc}} = 1.6\tau_{21}(1 + 0.05\xi^{1.5})^{-1} \quad (\text{B16})$$

for escape from a moving infinite slab, where $\xi = 0.90v_{\text{bulk}}/v_{\text{D}}$, v_{bulk} is the velocity difference between the center and the edge of the slab, and $v_{\text{D}} = \sqrt{2kT/m_{\text{H}}}$. Here, as v_{bulk} , we take the velocity at the edge of the central core region whose radius is R_c . Then $v_{\text{bulk}} = R_c/3t_{ff}$.

For other atomic lines, we take

$$N_{\text{esc}} = \begin{cases} 1.6\tau_{ul} & \text{for } \tau_{ul} < 10^4 \\ 160\tau_{ul}^{1/2} & \text{for } \tau_{ul} > 10^4 \end{cases} \quad (\text{B17})$$

(e.g., Elitzur & Ferland 1986). The optical depth averaged over a line is given by

$$\tau_{ul} = \frac{A_{ul}c^3}{8\pi\nu_{ul}^3} [n_l(\text{H})g_u/g_l - n_u(\text{H})]l_{\text{sh}}/v_{\text{D}}. \quad (\text{B18})$$

In order to take into account the effect of velocity gradient, we reduce the shielding length l_{sh} for lines other than Ly α in the case of large velocity gradient as

$$l_{\text{sh}} = \min(R_{\text{c}}, \Delta s_{\text{th}}) \quad (\text{B19})$$

where

$$\Delta s_{\text{th}} = v_{\text{D}} / \left(\frac{dv}{dr} \right) = 3v_{\text{D}}t_{\text{ff}}. \quad (\text{B20})$$

Recall that the correction for velocity gradient has been already included in the expression (B16) for Ly α photons. Then we take $l_{\text{sh}} = R_{\text{c}}$ for the Ly α line.

B.2. Molecular Hydrogen Lines

The radiative cooling rate Λ_{H_2} due to molecular hydrogen lines can be represented by the similar expression as equation (B1). We compute rovibrational population $n_{v,J}(\text{H}_2)$ of H_2 following Hollenbach & McKee (1979) using the renewed collisional rate coefficients given by Hollenbach & McKee (1989). We take the spontaneous radiative decay rates $A_{v,J,v',J'}$ from Turner, Kirby-Docken, & Dalgarno (1977). Also we take into account the effects of the external radiation by the same way as described for the atomic hydrogen lines (i.e., equation B5). The escape probability is given by (Takahashi, Hollenbach, & Silk 1983)

$$\beta_{\text{esc},ul} = [(1 - e^{-\tau_{ul}})/\tau_{ul}]e^{-\tau_a}, \quad (\text{B21})$$

for the case that the velocity is proportional to the radius. We consider the first three vibrational states ($v = 0 - 2$) with rotational levels up to $J = 20$ in each vibrational state. We assume the ortho to para ratio of molecular hydrogen to be the equilibrium value 3:1. We use the rovibrational energies $E(v, J)$ of Borysow, Frommhold, & Moraldi (1989).

B.3. Compton Coupling

The cooling rate of a gas with electron density n_e and temperature T embedded in a black body radiation field of energy density u and temperature T_γ is given by (Kompaneets 1957; Weymann

1965)

$$\Lambda_{\text{Compt}} = \frac{4k(T - T_\gamma)}{m_e c^2} c \sigma_T n_e u \quad (\text{ergs s}^{-1} \text{cm}^{-3}) \quad (\text{B22})$$

$$= \frac{16k\sigma_T \sigma_B n_e}{m_e c^2} T_\gamma^4 (T - T_\gamma) \quad (\text{ergs s}^{-1} \text{cm}^{-3}), \quad (\text{B23})$$

where σ_T is the Thomson cross section, σ_B is the Stefan-Boltzmann constant, and m_e is the mass of an electron. In order to treat the situation that the Compton energy transfer and continuum processes coexist both in optically thin and thick cases, we deal with the Compton process as if it was one of continuum sources, denoting

$$\kappa_{\text{Compt}}(\nu) = \frac{4kT_\gamma}{m_e c^2} \sigma_T n_e = a_{\text{Compt}} T_\gamma, \quad (\text{B24})$$

and

$$\eta_{\text{Compt}}(\nu) = \frac{4kT}{m_e c^2} \sigma_T n_e J(\nu) = a_{\text{Compt}} T J(\nu), \quad (\text{B25})$$

where $a_{\text{Compt}} \equiv (4k/m_e c^2) \sigma_T n_e$. This method reproduces the correct behavior both in optically thin and thick limit (Note that $T_\gamma = T$ in the optically thick limit). In evaluating the radiation temperature in the above equation, we use the definition

$$T_\gamma \equiv (\pi J / \sigma_B)^{1/4}, \quad (\text{B26})$$

where the mean intensity $J = \int J(\nu) d\nu$.

B.4. Continuum

We consider the following continuum processes (cf., Lenzuni et al. 1991). Among pure absorption, bound-free absorption of H, He, H^- , H_2^+ , free-free absorption of H^- , H, H_2 collision-induced absorption,⁸ and among scattering, Rayleigh scattering of H, and Thomson scattering are included. The cross sections are listed in Table 1.

The net rate of energy transport from matter to radiation per unit volume per unit frequency is

$$\Lambda_{\text{cont}}(\nu) = 4\pi[\eta_{\text{a}}(\nu) - \kappa_{\text{a}}(\nu)J(\nu)], \quad (\text{B27})$$

where $\eta_{\text{a}}(\nu)$ is the thermal part of the emission coefficient and $\kappa_{\text{a}}(\nu)$ is the true absorption coefficient. Also, we use the scattering coefficient $\kappa_{\text{s}}(\nu)$ below. Specifically,

$$\eta_{\text{a}}(\nu) = \sum_{\text{aj}=\text{a1}}^{\text{a8}} \eta_{\text{aj}}(\nu) \quad (\text{B28})$$

⁸Two-photon emission of atomic hydrogen was treated as described in §A.1.

and

$$\kappa_a(\nu) = \sum_{aj=a1}^{a8} \kappa_{aj}(\nu), \quad \kappa_s(\nu) = \kappa_{s1}(\nu) + \kappa_{s2}(\nu). \quad (\text{B29})$$

We assume that the radiation field is static inside the cloud, then

$$\Lambda_{\text{cont}}(\nu) = \frac{u(\nu) - u_{\text{ex}}(\nu)}{t_{\text{esc}}(\nu)}, \quad (\text{B30})$$

where $u(\nu)$ and $u_{\text{ex}}(\nu)$ are the radiation energy density in side and outside the cloud. The photon escape time

$$t_{\text{esc}}(\nu) = \frac{x(\nu)}{\chi(\nu)c}, \quad (\text{B31})$$

where the extinction coefficient

$$\chi(\nu) = \kappa_a(\nu) + \kappa_s(\nu), \quad (\text{B32})$$

and

$$x(\nu) \equiv \max[\tau(\nu)^2, \tau(\nu)], \quad (\text{B33})$$

by using optical depth $\tau(\nu) = \chi(\nu)R_c$. Equating equations (B27) and (B30), and using $u(\nu) = 4\pi J(\nu)/c$, we obtain

$$J(\nu) = \frac{J_{\text{ex}}(\nu) + \xi(\nu)x(\nu)S_a(\nu)}{1 + \xi(\nu)x(\nu)}, \quad (\text{B34})$$

where $\xi(\nu) \equiv \kappa_a(\nu)/\chi(\nu)$. The external radiation field $J_{\text{ex}}(\nu) = J_{\text{UV}}(\nu) + B(\nu; T_{\text{CMBR}})$ in our case, where T_{CMBR} is the temperature of the CMBR. If we include the Compton energy transfer, substituting

$$\frac{\eta_a(\nu) + \eta_{\text{Compt}}(\nu)}{\kappa_a(\nu) + \kappa_{\text{Compt}}(\nu)} = \frac{\eta_a(\nu) + a_{\text{Compt}}TJ(\nu)}{\kappa_a(\nu) + a_{\text{Compt}}T_\gamma} \quad (\text{B35})$$

into equation (B34) instead of $S_a(\nu)$, we obtain the final expression for the mean intensity inside the cloud:

$$J(\nu) = \frac{J_{\text{ex}}(\nu) + \xi(\nu)x(\nu)\eta_a(\nu)/(\kappa_a(\nu) + a_{\text{Compt}}T_\gamma)}{1 + \xi(\nu)x(\nu)[1 - a_{\text{Compt}}T/(\kappa_a(\nu) + a_{\text{Compt}}T_\gamma)]}. \quad (\text{B36})$$

Substituting equation (B36) into (B27) and integrating over frequency ν , we obtain the sum of cooling rates $\Lambda_{\text{cont}} + \Lambda_{\text{Compt}}$ due to the continuum and the Compton coupling.

In the following, we describe how to calculate the emission and absorption coefficients using the cross sections.

B.4.1. bound-free absorption / free-bound emission (a1-a4)

Consider the radiative association RA(i) of species A and B into i th state of C, whose binding energy is $h\nu_i$, and resultant free-bound emission,



and its inverse reaction PD(*i*) (i.e., photodissociation of C from *i*th state, or the bound-free absorption). The cross section of this (and its inverse) reaction is $\sigma_{\text{RA}i}(v)$ ($\sigma_{\text{PD}i}(\nu)$, respectively). In our case, the species C means H, He, H^- , and H_2^+ for the processes a1-a4, respectively.

From the Milne relation (e.g., Rybicki & Lightman 1979),

$$\sigma_{\text{RA}i} = \sigma_{\text{PD}i} \left(\frac{h\nu}{m_{\text{r}}c\nu} \right)^2 \frac{2g_{\text{C}i}}{z_{\text{A}}z_{\text{B}}}, \quad (\text{B38})$$

where the reduced mass $m_{\text{r}} = m_{\text{A}}m_{\text{B}}/m_{\text{C}}$, z_{A} (z_{B}) is the partition function of A (B, respectively), $g_{\text{C}i}$ is the statistical weight of the *i*th state of C, and

$$\frac{1}{2}m_{\text{r}}v^2 = h(\nu - \nu_i). \quad (\text{B39})$$

The emission coefficient of RA(*i*) is given by

$$\eta_{\text{RA}i}(\nu) = \frac{h\nu}{4\pi} \sigma_{\text{RA}i} n(\text{A})n(\text{B})v f(v) \frac{dv}{d\nu} \quad (\text{B40})$$

$$= \frac{2h\nu^3}{c^2} \frac{g_{\text{C}i}}{z_{\text{A}}z_{\text{B}}} \left(\frac{h^2}{2\pi m_{\text{r}}kT} \right)^{3/2} \sigma_{\text{PD}i} \exp\left(-\frac{h(\nu - \nu_i)}{kT}\right) n(\text{A})n(\text{B}), \quad (\text{B41})$$

where the distribution function of the relative velocity between particles A and B

$$f(v) = 4\pi \left(\frac{m_{\text{r}}}{2\pi kT} \right)^{3/2} \exp\left(-\frac{m_{\text{r}}v^2}{2kT}\right) v^2. \quad (\text{B42})$$

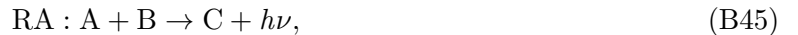
Also, the absorption coefficient of PD(*i*) is given by

$$\kappa_{\text{PD}i}(\nu) = \sigma_{\text{PD}i} n_i(\text{C}) - \frac{h\nu}{4\pi} \frac{c^2}{2h\nu^3} \sigma_{\text{RA}i} n(\text{A})n(\text{B})v f(v) \frac{dv}{d\nu} \quad (\text{B43})$$

$$= \sigma_{\text{PD}i} n_i(\text{C}) - \frac{g_{\text{C}i}}{z_{\text{A}}z_{\text{B}}} \left(\frac{h^2}{2\pi m_{\text{r}}kT} \right)^{3/2} \sigma_{\text{PD}i} \exp\left(-\frac{h(\nu - \nu_i)}{kT}\right) n(\text{A})n(\text{B}). \quad (\text{B44})$$

The second term in the equation above represents the induced association.

Summing over all levels, we obtain the emission and absorption coefficient owing to the reaction



and its inverse PD;

$$\eta_{\text{RA}}(\nu) = \sum_i \eta_i(\nu) \quad (\text{B46})$$

$$= \frac{2h\nu^3}{c^2} \sigma_{\text{PD}}^* n(\text{C}) \exp\left(-\frac{h\nu}{kT}\right) \left[K(T)^{-1} \frac{n(\text{A})n(\text{B})}{n(\text{C})} \right], \quad (\text{B47})$$

and

$$\kappa_{\text{PD}}(\nu) = \sum_i \kappa_i(\nu) \quad (\text{B48})$$

$$= \sigma_{\text{PD}} n(\text{C}) \left\{ 1 - \exp\left(-\frac{h\nu}{kT}\right) \left[\frac{\sigma_{\text{PD}}^*}{\sigma_{\text{PD}}} K(T)^{-1} \frac{n(\text{A})n(\text{B})}{n(\text{C})} \right] \right\}. \quad (\text{B49})$$

In the above equations, the equilibrium constant

$$K(T) \equiv \left[\frac{n(\text{A})n(\text{B})}{n(\text{C})} \right]^* \quad (\text{B50})$$

$$= \frac{z_{\text{A}}z_{\text{B}}}{z_{\text{C}}} \left(\frac{2\pi m_{\text{r}}kT}{h^2} \right)^{3/2} \exp\left(-\frac{h\nu_1}{kT}\right), \quad (\text{B51})$$

and

$$\sigma_{\text{PD}} = \sum_i c_i \sigma_{\text{PD}i}, \quad \sigma_{\text{PD}}^* = \sum_i c_i^* \sigma_{\text{PD}i}, \quad (\text{B52})$$

where the relative population of level i is $c_i = n_i(\text{C})/n(\text{C})$, and its LTE value $c_i^* = g_{\text{C}i} \exp(-h(\nu_1 - \nu_i)/kT)/z_{\text{C}}$.

B.4.2. free-free absorption/ emission (a5,a6) and H₂ collision-induced absorption/ emission (a7,a8)

First, we consider the free-free emission and absorption (a5,a6)



where A=H, and H⁺ for the processes a5, and a6, respectively. The absorption cross section for A is σ_{FF} . Note that $\sigma_{\text{FF}} \propto n(e)$ (see Table 1). This process is collisional, then it occurs at the LTE rate. Thus,

$$\eta_{\text{FF}}(\nu) = \frac{2h\nu^3}{c^2} \sigma_{\text{FF}} n(\text{A}) \exp\left(-\frac{h\nu}{kT}\right), \quad (\text{B54})$$

and

$$\kappa_{\text{FF}}(\nu) = \sigma_{\text{FF}} n(\text{A}) \left\{ 1 - \exp\left(-\frac{h\nu}{kT}\right) \right\}. \quad (\text{B55})$$

Next, we consider the H₂ collision-induced emission and absorption (a7,a8)



In this equation, B means H₂ for the process a7, and He for a8. The absorption cross section for H₂ is σ_{CI} . This process occurs only at so high density that $\sigma_{\text{CI}} = \sigma_{\text{CI}}^*$. Then, in the same way as the above,

$$\eta_{\text{CI}}(\nu) = \frac{2h\nu^3}{c^2} \sigma_{\text{CI}} n(\text{H}_2) \exp\left(-\frac{h\nu}{kT}\right), \quad (\text{B57})$$

and

$$\kappa_{\text{CI}}(\nu) = \sigma_{\text{CI}} n(\text{H}_2) \left\{ 1 - \exp\left(-\frac{h\nu}{kT}\right) \right\}. \quad (\text{B58})$$

B.4.3. scattering (s1,s2)

We denote the cross section of A for the scattering (s1,s2)

$$\text{SC} : \text{A} + \gamma \leftrightarrow \text{A} + \gamma' \quad (\text{B59})$$

as $\sigma_{\text{SC}}(\nu)$. In the above expression, A=H, and e for the scattering s1, and s2, respectively. The scattering coefficient is given by

$$\kappa_{\text{SC}}(\nu) = \sigma_{\text{SC}}(\nu)n(\text{A}). \quad (\text{B60})$$

C. Chemical Reactions

We treat non-equilibrium chemistry of hydrogen-helium gas between the following nine species: H, H₂, e , H⁺, H₂⁺, H⁻, He, He⁺, and He⁺⁺. Included reactions and their rate coefficients are presented in Table 2.

When the gas density rises, and consequently the chemical reaction timescale becomes shorter than the collapse timescale of the cloud, the chemical equilibrium is reached. In addition to this, if the cloud becomes optically thick to the continuum, and as a result, the radiation field reduces to the black body radiation of the matter temperature, the chemical equilibrium reduce to the Saha value. In order to reproduce this feature, inverse processes are included for all reactions. Rates of inverse reactions are computed from the principle of detailed balance.

We switch to equilibrium chemistry at a sufficiently high density n_{eq} where Saha equilibrium has been already reached. In our case, $n_{\text{eq}} = 10^{18-19} \text{cm}^{-3}$.

The rate coefficients of the radiative association

$$\text{RA} : \text{A} + \text{B} \rightarrow \text{C} + \gamma, \quad (\text{C1})$$

and its inverse reaction PD, i.e. the photodissociation of C, can be written as

$$k_{\text{RA}} = K(T)^{-1} \int_0^\infty \frac{4\pi B(\nu; T)}{h\nu} \sigma_{\text{PD}}^* [1 - \exp(-\frac{h\nu}{kT})] d\nu, \quad (\text{C2})$$

and

$$k_{\text{PD}} = \int_0^\infty \frac{4\pi J(\nu)}{h\nu} \sigma_{\text{PD}} \{1 - \exp(-\frac{h\nu}{kT}) [\frac{\sigma_{\text{PD}}^*}{\sigma_{\text{PD}}} K(T)^{-1} \frac{n(\text{A})n(\text{B})}{n(\text{C})}]\} d\nu. \quad (\text{C3})$$

from the discussion in §A 4.1.

The partition function of H

$$z_{\text{H}} = \sum_{n=1}^5 g_n \exp(-E_n/kT) \quad (\text{C4})$$

where $g_n = 2n^2$ and $E_n = 13.598\text{eV}/n^2$. For H_2 , the sum extends over $0 \leq v \leq 5$ and $0 \leq J \leq 25$. The rovibrational energies $E(v, J)$ are taken from Borysow et al.(1989). The partition function of H_2^+ is taken from Patch & McBride (1968). For other species, we take $z_e = 2$, $z_{\text{H}^+} = 1$, $z_{\text{H}^-} = 1$, $z_{\text{He}} = 1$, $z_{\text{He}^+} = 2$, and $z_{\text{He}^{++}} = 1$.

REFERENCES

- Abel, T., Bryan G. L., & Norman M. L. 2000, *ApJ*, 540, 39
- Black, J. H. 1981, *MNRAS*, 197, 553
- Bonilha, J. R. M., Ferch, R., Salpeter, E. E., Slater, G., & Noerdlinger, P. D. 1979, *ApJ*, 233, 649
- Borysow, A., Jørgensen, U. G., & Zheng, C. 1997, *A&A*, 324, 185
- Borysow, A., Frommhold, L., & Moraldi, M. 1989, *ApJ*, 336, 495
- Bromm, V., Coppi, P. S., & Larson, R. B. 1999, *ApJ*, 527, L5
- Carlberg, R. G. 1981, *MNRAS*, 197, 1021
- Ciardì, B., Ferrara, A., & Abel, T. 2000, *ApJ*, 533, 594
- de Jong, T., Dalgarno, A., & Boland, W. 1980, *A&A*, 91, 68
- Doroshkevich, A. G., & Kolesnik I. G. 1976, *Soviet Astron.*, 20, 4
- Draine, B. T., & Bertoldi, F. 1996, *ApJ*, 468, 269
- Drawin, H. W. 1969, *Zs. Phys.*, 225, 483
- Elitzur, M., & Ferland, G. J. 1986, *ApJ*, 305, 35
- Fuller, T. M., & Couchman, H. M. P. 2000, *ApJ*, 544, 6
- Galli, D., & Palla, F. 1998, *A&A*, 335, 403
- Haiman, Z., Thoul, A. A., & Loeb, A. 1996, *ApJ*, 464, 523
- Haiman, Z., Rees, M. J., & Loeb, A. 1997, *ApJ*, 476, 458; erratum 484, 985
- Hollenbach, D., & McKee, C. F. 1979, *ApJS*, 41, 555
- Hollenbach, D., & McKee, C. F. 1989, *ApJ*, 342, 306
- Inutsuka, S., & Miyama, S. M. 1997, *ApJ*, 480, 681
- Izotov, Yu. I., & Thuan, T. X. 1998, *ApJ*, 500, 188

- Janey, R. K., Langer, W. D., Evans, K., Jr., & Post, D. E., Jr. 1987, *Elementary Processes in Hydrogen-Helium Plasmas* (Berlin: Springer-Verlag)
- John, T. L. 1988, *A&A*, 193, 189
- Kashlinsky, A. & Rees, M. J. 1983, *MNRAS*, 205, 955
- Kompaneets, A. S. 1957, *Soviet Phys. JETP* 4, 730
- Kurucz, R. L. 1970, *Smithsonian Obs. Special Report*, No.309
- Larson, R. B. 1969, *MNRAS*, 145, 271
- Lenzuni, P., Chernoff, D. F., & Salpeter, E. E. 1991, *ApJS*, 76, 759
- Mac Low, M.-M., & Ferrara, A. 1999, *ApJ*, 513, 142
- Masunaga, H., & Inutsuka, S. 1999, *ApJ*, 510, 822
- Matsuda, T., Sato, H., & Takeda, H. 1969, *Prog. Theor. Phys.*, 42, 219
- Nakamura, F., & Umemura, M. 1999, *ApJ*, 515, 239
- Omukai, K., & Nishi, R. 1998, *ApJ*, 508, 141
- Omukai, K., & Nishi, R. 1999, *ApJ*, 518, 64
- Osterbrock, D. E. 1989, *Astrophysics of Gaseous Nebulae and Active Galactic Nuclei* (Mill Valley: University Science Books)
- Ostriker, J. P., & Gnedin N. Y. 1996, *ApJ*, 472, L63
- Palla, F., Salpeter, E. E., & Stahler, S. W. 1983, *ApJ*, 271, 632
- Patch, R. W., & McBride, B. J. 1968, *NASA Technical Note D-4523*
- Padmanabhan, T., 1993, *Structure Formation in the Universe* (Cambridge: Cambridge University Press)
- Peebles, P. J. E., & Dicke, R. H., 1968, *ApJ*, 154, 891
- Penston, M. V. 1969, *MNRAS*, 144, 425
- Rybicki, G. B., & Lightman, A. P. 1979, *Radiative Processes in Astrophysics* (New York: Wiley)
- Saslaw, W. C., & Zipoy, D. 1967, *Nature*, 216, 976
- Shapiro P. R., & Kang, H. 1987, *ApJ*, 318, 32

- Sobelman, I. I., Vainshtein, L. A., & Yukov, E. A. 1981, *Excitation of Atoms and Broadening of Spectral Lines* (Berlin: Springer-Verlag)
- Spitzer, L., Jr., & Greenstein, J. L. 1951, *ApJ*, 114, 407
- Stahler, S. W., Shu, F. H., & Taam, R. E. 1980, *ApJ*, 241, 637
- Stancil, P. C. 1994, *ApJ*, 430, 360
- Susa, H., & Kitayama, T. 2000, *MNRAS*, 317, 175 preprint astro-ph/0004303
- Takahashi, T., Hollenbach, D. J., & Silk, J. 1983, *ApJ*, 275, 145
- Tegmark, M., Silk, J., Rees, M. J., Blanchard, A., Abel, T., & Palla, F. 1997, *ApJ*, 474, 1
- Tielens, A. G. G. M., & Hollenbach, D. 1985, *ApJ*, 291, 722
- Turner, J., Kirby-Docken, K., & Dalgarno, A. 1977, *ApJS*, 35, 281
- Uehara, H., Susa, H., Nishi, R., Yamada, M., & Nakamura, T. 1996, *ApJ*, 473, L95
- Weymann, R. 1965, *Phys. Fluids*, 8, 2112
- Wolfire, M. G., & Cassinelli, J. P. 1987, *ApJ*, 319, 850
- Yahil, A. 1983, *ApJ*, 265, 1047
- Yamada, M., & Nishi, R. 1998, *ApJ*, 505, 148
- Yoneyama, T. 1972, *PASJ*, 24, 87

Table 1. Continuum Processes

number	name	process	cross section (cm ²)
a1	H b-f	$\text{H}(n) + \gamma \rightarrow \text{H}^+ + e$	$7.909 \times 10^{-18} n(\nu/\nu_n)^{-3}$ $h\nu_n = 13.598\text{eV}/n^2$
a2	He b-f	$\text{He} + \gamma \rightarrow \text{He}^+ + e$	$7.83 \times 10^{-18} [1.66(\nu/\nu_T)^{-2.05} - 0.66(\nu/\nu_T)^{-3.05}]$, $h\nu_T = 24.586\text{eV}$
a3	H ⁻ b-f	$\text{H}^- + \gamma \rightarrow \text{H} + e$	$10^{-18} \lambda^3 (1/\lambda - 1/\lambda_0)^{3/2} f(\lambda)$, $\lambda_0 = 1.6419\mu\text{m}$ $f(\lambda)$ given by Eq.(5) of ref.
a4	H ₂ ⁺ b-f	$\text{H}_2^+ + \gamma \rightarrow \text{H} + \text{H}^+$	see Table 2 of ref.
a5	H ⁻ f-f	$\text{H} + e + \gamma \rightarrow \text{H} + e$	$k_\lambda^{\text{ff}}(T) k_B T n_e$ $k_\lambda^{\text{ff}}(T)$ given by Eq.(6) of ref.
a6	H f-f	$\text{H}^+ + e + \gamma \rightarrow \text{H}^+ + e$	$3.692 \times 10^8 g_{\text{ff}}(\nu, T) \nu^{-3} T^{-1/2} n_e$, we take $g_{\text{ff}}(\nu, T) = 1$
a7	H ₂ -H ₂ CIA	$\text{H}_2(v, J) + \text{H}_2 + \gamma \rightarrow \text{H}_2(v', J') + \text{H}_2$	see Fig.1 of ref.
a8	H ₂ -He CIA	$\text{H}_2(v, J) + \text{He} + \gamma \rightarrow \text{H}_2(v', J') + \text{He}$	see Fig.2 of ref.
s1	H Rayleigh	$\text{H} + \gamma \rightarrow \text{H} + \gamma'$	$5.799 \times 10^{-29} \lambda^{-4} + 1.422 \times 10^{-30} \lambda^{-6}$ $+ 2.784 \times 10^{-32} \lambda^{-8}$
s2	Thomson	$e + \gamma \rightarrow e + \gamma'$	6.65×10^{-25}

Note. — The wavelength λ is in μm .

References. — (1) Rybicki & Lightman (1979), (2) Osterbrock (1989), (3) John (1988), (4) Stancil (1994), (5) Borysow et al. (1997), (6) Kurucz (1970)

Table 2. Chemical Reactions

Number	Reaction	Rate Coefficient	Reference
1,2	$\text{H}(n) + e \rightleftharpoons \text{H}^+ + 2e$	$k_1 = \sum_{n=1}^5 c_n k_{1,n}$ $k_{1,n=1} = 4.25 \times 10^{-11} T^{1/2} \exp(-\chi_H/kT)$ $k_{1,n=2} = 6.69 \times 10^{-10} T^{1/2} \exp(-\chi_H/2^2/kT)$ ($T < 4680\text{K}$) $k_{1,n=2}$: see Janev et al. [2.1.6] ($T > 4680\text{K}$) $k_{1,n \geq 3} = 9.56 \times 10^{-6} T(\text{eV})^{-1.5}$ $(\beta_n^{2.33} + 4.38\beta_n^{1.72} + 1.32\beta_n)^{-1} \exp(-\beta_n)$, $\beta_n = (\chi_H/n^2)/kT$ $k_2 = k_1^*(z_H/z_{H^+}z_e)4.1414 \times 10^{-16} T^{-1.5} \exp(\chi_H/kT)$ $k_1^* = \sum_{n=1}^5 c_n^* k_{1,n}$	1 1 2
3,4	$\text{H}(n) + \text{H} \rightleftharpoons \text{H}^+ + e + \text{H}$	$k_3 = \sum_{n=1}^5 c_n k_{3,n}$ $k_{3,1} = 1.2 \times 10^{-17} T^{1.2} \exp(-\chi_H/kT)$ $k_{3,n \geq 2} = 7.86 \times 10^{-15} n^4 f_n T^{0.5} (1 + 1.27 \times 10^{-5} n^2 T)$ $(1 + 4.76 \times 10^{-17} n^4 T^2)^{-1} \exp(-\chi_H/n^2/kT)$ $f_2 = 0.71, f_3 = 0.81, f_4 = 0.94$ $k_4 = k_3^*(z_H/z_{H^+}z_e)4.1414 \times 10^{-16} T^{-1.5} \exp(\chi_H/kT)$ $k_3^* = \sum_{n=1}^5 c_n^* k_{3,n}$	1 3
5,6	$\text{H}^- + \text{H}^+ \rightleftharpoons \text{H}(n) + \text{H}$	$k_5 = \sum_{n=1}^3 k_{5,n}$ $k_{5,1} = 6.92 \times 10^{-14} T^{0.5}$ $k_{5,2} = 8.0 \times 10^{-13} T^{0.83}$ $k_{5,3} = 6.18 \times 10^{-7} T^{-0.27}$ $k_6 = [\sum_{n=1}^3 (c_n/c_n^*) k_{5,n}]$ $(z_{\text{H}^-} z_{\text{H}^+} / z_{\text{H}^2}) \exp[-(\chi_{\text{H}} - \chi_{\text{H}^-})/kT]$	1
7,8	$\text{H}_2 + \text{H}^+ \rightleftharpoons \text{H} + \text{H}_2^+$	$k_7 = 1.5 \times 10^{-10} \exp(-1.4 \times 10^4/T)$ ($T > 10^4\text{K}$) $k_7 = 3 \times 10^{-10} \exp[-(\chi_{\text{H}_2} - \chi_{\text{H}_2^+})/kT]$ ($T < 10^4\text{K}$) $k_8 = k_7 (z_{\text{H}^+} z_{\text{H}_2} / z_{\text{H}} z_{\text{H}_2^+}) \exp[(\chi_{\text{H}_2} - \chi_{\text{H}_2^+})/kT]$	4
9,10	$\text{H} + \text{H}^- \rightleftharpoons \text{H}_2 + e$	$k_9 = 1.5 \times 10^{-9}$ ($T < 3 \times 10^2\text{K}$) $k_9 = 4.0 \times 10^{-9} T^{-0.17}$ ($T > 3 \times 10^2\text{K}$) $k_{10} = k_{10,\text{H}}^{1-a} k_{10,\text{L}}^a$ $k_{10,\text{L}} = 2.7 \times 10^{-8} T^{-1.27} \exp[-(\chi_{\text{H}_2} - \chi_{\text{H}^-})/kT]$	4 4

Table 2—Continued

Number	Reaction	Rate Coefficient	Reference
		$k_{10,H} = k_9(z_H z_{H^-} / z_{H_2} z_e) 2.775 \times 10^4 \exp[-(\chi_{H_2} - \chi_{H^-})/kT]$ $a = (1 + n/n_{cr})^{-1}$ $\log_{10}(n_{cr}) = 4.0 - 0.416 \log_{10}(T/10^4)$ $-0.327(\log_{10}(T/10^4))^2$	5
11,12	$H_2^+ + e \rightleftharpoons H(n) + H$	$k_{11} = \sum_{n=1}^5 k_{11,n} = 2 \times 10^{-7} T^{-1/2}$ $k_{11,1} : k_{11,2} : k_{11,3} : k_{11,4} : k_{11,5} = 0 : 0.10 : 0.45 : 0.22 : 0.12$ but, $k_{11,n} = 0$ in case of $\chi_H - \chi_{H_2^+} - \chi_H/n^2 < kT$ $k_{12} = [\sum_{n=1}^5 (c_n/c_n^*) k_{11,n}]$ $(z_{H_2^+} z_e / z_H^2) 3.6034 \times 10^{-5} \exp[-(\chi_H - \chi_{H_2^+})/kT]$	4 2
13,14	$2H_2 \rightleftharpoons 2H + H_2$	$k_{13} = k_{13,H}^{1-a} k_{13,L}^a$ $k_{13,L} = 1.18 \times 10^{-10} \exp(-6.95 \times 10^4/T)$ $k_{13,H} = 1.30 \times 10^{-9} \exp(-5.33 \times 10^4/T)$ $a = (1 + n/n_{cr})^{-1}$ $\log_{10}(n_{cr}) = 4.845 - 1.3 \log_{10}(T/10^4)$ $+1.62(\log_{10}(T/10^4))^2$ $k_{14} = k_{13,H}(z_{H_2}/z_H^2) 1.493 \times 10^{-20} T^{-1.5} \exp(\chi_{H_2}/kT)$	5
15,16	$H_2 + H \rightleftharpoons 3H$	$k_{15} = k_{15,H}^{1-a} k_{15,L}^a$ $k_{15,L} = 1.12 \times 10^{-10} \exp(-7.035 \times 10^4/T)$ $k_{15,H} = 6.5 \times 10^{-7} T^{-1/2}$ $\exp(-\chi_{H_2}/kT)[1 - \exp(-6000/T)]$ $a = (1 + n/n_{cr})^{-1}$ $\log_{10}(n_{cr}) = 4.0 - 0.416 \log_{10}(T/10^4)$ $-0.327(\log_{10}(T/10^4))^2$ $k_{16} = k_{15,H}(z_{H_2}/z_H^2) 1.493 \times 10^{-20} T^{-1.5} \exp(\chi_{H_2}/kT)$	5 6 5
17,18	$H_2 + e \rightleftharpoons 2H + e$	$k_{17} = 1.3 \times 10^{-18} T^2 \exp(-\chi_{H_2}/kT)$ $k_{18} = k_{17}(z_{H_2}/z_H^2) 1.493 \times 10^{-20} T^{-1.5} \exp(\chi_{H_2}/kT)$	1
19,20	$H^- + e \rightleftharpoons H + 2e$	$k_{19} = 4 \times 10^{-12} T \exp(-\chi_{H^-}/kT)$ $k_{20} = k_{19}(z_{H^-} / z_H z_e) 4.1414 \times 10^{-16} T^{-1.5} \exp(\chi_{H^-}/kT)$	5

Fig. 1.— Two FUV spectra studied in this work. The solid and dotted lines indicate those of Types a and b, respectively. The normalization of intensity $J_{21} = 1$ for both types. Also shown are the threshold frequency of H^- photodissociation (0.755 eV) and a representative value of Lyman and Werner (LW) bands (12.4 eV).

Fig. 2.— The density-temperature relation for the collapse of primordial clouds irradiated with FUV radiation. The spectra are type a: $J_{\text{UV}}(\nu) = J_{21} \times 10^{-21}(\nu/\nu_{\text{th}})^{-1}$. The evolutionary trajectories are drawn for $J_{21} = 0, 10^{-2}, 1, 10^2, 10^4$, and 10^5 . The trajectories for $J_{21} > 10^5$ are identical to that for $J_{21} = 10^5$. The dashed lines indicate the constant Jeans mass. The dark matter gravity is neglected in calculating the Jeans masses.

Fig. 3.— Same as Fig. 2, but for spectra type b: $J_{\text{UV}}(\nu) = J_{21} \times 10^{-21}[B(\nu; 10^4\text{K})/B(\nu_{\text{th}}; 10^4\text{K})]$ ($\nu < \nu_{\text{th}}$). The evolutionary trajectories are drawn for $J_{21} = 0, 10^{-2}, 1, 10^2$, and 10^3 . The trajectories for $J_{21} > 10^3$ are identical to that for $J_{21} = 10^3$.

Fig. 4.— Concentration of (a) hydrogen molecules $y(\text{H}_2)$ and (b) electrons $y(e)$ for the clouds irradiated with the power-law type radiation (type a spectrum in the text) with $J_{21} = 10^5$ (*solid lines*), 10^4 (*dotted lines*), 10^2 (*short-dashed lines*), 1 (*long-dashed lines*), 10^{-2} (*dash-dotted lines*), and 0 (*long-dash-dotted lines*).

Fig. 5.— Cooling/heating rates per unit baryonic mass as a function of the central number density for the clouds irradiated with the power-law type radiation of (a) $J_{21} = 0$, (b) 10^4 and (c) 10^5 . These include the contributions by the compression, chemical reactions, atomic hydrogen lines, H two-photon emission, continuum, and H_2 lines. The dominant continuum processes are (a) H^- free-bound emission ($n \lesssim 10^{11.5}\text{cm}^{-3}$), H_2 collision-induced emission ($10^{11.5}\text{cm}^{-3} \lesssim n$); (b) H^- free-bound emission ($n \lesssim 10^{11.5}\text{cm}^{-3}$), H_2 collision-induced emission ($10^{11.5}\text{cm}^{-3} \lesssim n$); and (c) H^- free-free emission ($10^2 \lesssim n \lesssim 10^{4.5}\text{cm}^{-3}$), H^- free-bound emission ($10^{4.5}\text{cm}^{-3} \lesssim n$), respectively. The chemical reactions contributing dominantly to the cooling/heating rates are: (a) and (b): H_2 formation ($n \lesssim 10^{13}\text{cm}^{-3}$), H_2 dissociation ($10^{13} \lesssim n \lesssim 10^{15}\text{cm}^{-3}$), H_2 formation ($10^{15} \lesssim n \lesssim 10^{16}\text{cm}^{-3}$), H_2 dissociation ($10^{16} \lesssim n \lesssim 10^{21}\text{cm}^{-3}$), H ionization ($10^{21}\text{cm}^{-3} \lesssim n$), and (c) H_2 formation ($n \lesssim 10^{15.5}\text{cm}^{-3}$), H_2 dissociation ($10^{15.5} \lesssim n \lesssim 10^{16.5}\text{cm}^{-3}$), H ionization ($10^{16.5}\text{cm}^{-3} \lesssim n$), respectively (cf. Fig.4).

Fig. 6.— Estimated H_2 fraction vs. the amount of H_2 needed for efficient H_2 cooling during the initial adiabatic temperature rise. We assume that the temperature rises adiabatically from the initial state of calculation, that is, $T = T_0(n/n_0)^{2/3}$, where $T_0 = 39$ K, and $n_0 = 8.9 \times 10^{-2}\text{cm}^{-3}$ are the initial temperature and number density, respectively. The ionization degree is taken to be 10^{-4} . The H_2 fractions are estimated by equation (A2). The solid and dotted lines illustrate the H_2 fractions for Types a and b FUV radiation whose values of J_{21} are indicated in the figure. The thick solid curve shows the necessary H_2 fraction for the cloud to cool in a free-fall time (eq. [A1])

Fig. 7.— Estimated H_2 fraction vs. the amount of H_2 needed for efficient H_2 cooling for clouds that collapse isothermally by atomic cooling. The temperature and ionization degree are taken to

Table 2—Continued

Number	Reaction	Rate Coefficient	Reference
21,22	$\text{H}_2^+ + e \rightleftharpoons \text{H} + \text{H}^+ + e$	$k_{21} = 2 \times 10^{-7} \exp(-\chi_{\text{H}_2^+}/kT)$ $k_{22} = k_{21}(z_{\text{H}_2^+}/z_{\text{H}}z_{\text{H}^+})1.493 \times 10^{-20}T^{-1.5} \exp(\chi_{\text{H}_2^+}/kT)$	1
23,24	$\text{He} + e \rightleftharpoons \text{He}^+ + 2e$	$k_{23} = 2.38 \times 10^{-11}T^{1/2}[1 + (T/10^5)]^{-1} \exp(-\chi_{\text{He}}/kT)$ $k_{24} = k_{23}(z_{\text{He}}/z_{\text{He}^+}z_e)4.1414 \times 10^{-16}T^{-1.5} \exp(\chi_{\text{He}}/kT)$	7
25,26	$\text{He}^+ + e \rightleftharpoons \text{He}^{++} + 2e$	$k_{25} = 5.68 \times 10^{-12}T^{1/2}[1 + (T/10^5)]^{-1} \exp(-\chi_{\text{He}^+}/kT)$ $k_{26} = k_{25}(z_{\text{He}^+}/z_{\text{He}^{++}}z_e)4.1414 \times 10^{-16}T^{-1.5} \exp(\chi_{\text{He}^+}/kT)$	7
27,28	$\text{H} + \gamma \rightleftharpoons \text{H}^+ + e$	see equations (C2), (C3) in the text and process (a1) in Table 1	
29,30	$\text{He} + \gamma \rightleftharpoons \text{He}^+ + e$	see equations (C2), (C3) in the text and process (a2) in Table 1	
31,32	$\text{H}^- + \gamma \rightleftharpoons \text{H} + e$	see equations (C2), (C3) in the text and process (a3) in Table 1	
33,34	$\text{H}_2^+ + \gamma \rightleftharpoons \text{H} + \text{H}^+$	see equations (C2), (C3) in the text and process (a4) in Table 1	
35	$\text{H}_2 + \gamma \rightarrow \text{H}_2^* \rightarrow 2\text{H}$	$k_{35} = 1.4 \times 10^9 J(h\nu = 12.4\text{eV})f_{\text{sh}}$ $f_{\text{sh}} = \min [1, (N_{\text{H}_2}/10^{14}\text{cm}^{-2})^{-3/4}]$	8

Note. — The temperature T is in K, except otherwise noted.

Note. — The binding energies are $\chi_{\text{H}}/k = 1.578 \times 10^5\text{K}$, $\chi_{\text{H}_2}/k = 5.197 \times 10^4\text{K}$, $\chi_{\text{H}^-}/k = 8.761 \times 10^3\text{K}$, $\chi_{\text{H}_2^+}/k = 3.067 \times 10^4\text{K}$, $\chi_{\text{He}}/k = 2.853 \times 10^5\text{K}$, and $\chi_{\text{He}^+}/k = 6.312 \times 10^5\text{K}$.

References. — (1) Lenzuni et al. (1991), (2) Janev et al. (1987), (3) Drawin (1969), (4) Galli & Palla (1998), (5) Shapiro & Kang (1987), (6) Palla et al. (1983), (7) Black (1981), (8) Draine & Bertoldi (1996)

be 8000K and 10^{-4} , respectively. The H_2 fractions are estimated by eq.(A2). The solid and dotted lines illustrate the H_2 fractions for types *a* and *b* FUV radiation whose values of J_{21} are indicated in the figure. The thick solid curve shows the necessary H_2 fraction for the cloud to cool in a free-fall time (eq.[A1]).

